Scattering properties of the heterogeneous and non-spherical haze particles in the SWIR band

M Fan[1,2], L Chen[1,*], S Li[1], J Tao[1], L Su[1], M Zou[1,2], D Han[1], Y Zhang[1]

1 State Key Laboratory of Remote Sensing Science, Jointly Sponsored by the Institute of Remote Sensing and Digital Earth of Chinese Academy of Sciences and Beijing Normal University, Beijing 100101, China

2 University of Chinese Academy of Sciences, Beijing 100049, China

E-mail: lfchen@irsa.ac.cn (L Chen)

Abstract. To effectively estimate the influence of multiple scattering caused by haze particles on the misestimating of CO_2 concentrations, it is necessary to understand the scattering properties of haze particles in the shortwave infrared (SWIR) wavelength range (~1.6μm) using satellite data. Due to the complexity of structures and components of haze particles, this paper investigates effects of particle size and chemical component on the scattering properties of both single non-spherical particles and aggregates for the 1.6μm by using numerically effective medium theory and core-mantle theory. For the single non-spherical particles, the scattering parameters (e.g. scattering phase function, single scattering albedo, extinction coefficient and scattering coefficient) are calculated by combining the T-matrix method and the Maxwell-Garnett effective medium theory. For the aggregates, the particle-cluster aggregation algorithm is used to generate aggregates with different monomer numbers. And then, the Core-Mantle Generalized Multi-particle Mie (CMGMM) method is used to compute the scattering parameters. The results indicate that the scattering characteristics are significantly different for both single non-spherical particles and aggregates.

1. Introduction

Human activities, such as the burning of fossil fuels and the clearing of forests, have increased global carbon dioxide (CO_2) background concentration in the atmosphere by ~30% from a preindustrial level of 280 parts per million (ppm) to more than 370 ppm at present. Although in site measurements could provide highly accurate CO_2 concentration (~0.1 ppm), these observations (both vertical and horizontal) are too sparse to constrain their usefulness in models of CO_2 sources and sinks. The satellite measurement has an advantage of providing dense and uniform atmospheric CO_2 observations over land and ocean on a global scale. Some previous studies indicated that space-based CO_2 column observations have the potential benefit for estimating surface fluxes, i.e. source/sink quantification, if their global precisions are required in the range of 1–10 ppm (0.3–3.0%) and without significant biases [1-3]. However, the accuracy requirements for the satellite measurements of CO_2 face a large challenge in the Short Wavelength Infrared (SWIR) wavelength range (~1.6μm), because the multiple scattering of aerosols can influence the light path and therefore could introduce uncertainties in the retrieved CO_2 total column[4, 5].

During the last three decades, the rapid economic development has resulted in heavy atmospheric aerosol loadings in China, and brown haze events occur more frequently [6, 7]. It could contribute to

visibility reduction, and has severe adverse impacts on human health. The high aerosol loading over China may lead higher uncertainties into the estimation of light path, and may introduce a larger error into CO_2 retrieval algorithm for many regions of China. To effectively estimate the influence of the multiple scattering caused by haze particles on the misestimating for CO_2 retrieval, it is necessary to well understand the scattering properties of the haze particles in the SWIR band. It is often assumed that aerosol particles are spherical and homogeneous in many climate and remote sensing applications. However, some transmission electron microscopy observations have indicated that most of the particles in haze samples are heterogeneous and non-spherical, and are always covered by visible coatings [8-10]. Consequently, the assumptions of nonsphericity and heterogeneity should be taken into account when studying the scattering properties of haze particles in the SWIR band (1.6μm).

The scattering parameters of single non-spherical particle can be calculated by solving electromagnetic equations with rigorous methods like the T-matrix method [11] and the finite difference time domain (FDTD) method [12]. For fractal aggregates, two numerically accurate methods have been recently developed to predict their radiative properties: the cluster T-matrix method (CMT) [13] and the generalized multi-sphere Mie-solution (GMM) [14]. To simulate the scattering properties of heterogeneous particles, the effective medium theory (e.g. the Maxwell-Garnett rule, the Bruggeman rule and the coherent potential approximation rule) needs to be introduced into calculations [15]. Moreover, Xu and Khlebtsov extended the GMM method to compute the scattering properties of the aggregates with coated inhomogeneous monomers, referred as the Core-mantle GMM (CMGMM) method [16].

In this paper, in1.6μm wavelength, the effects of complex component on the scattering properties of both single non-spherical particles and aggregates are investigated using numerically effective medium theory and core-mantle theory. For the single non-spherical particles, the scattering parameters (e.g. scattering phase function, single scattering albedo, extinction coefficient and absorption coefficient) were calculated by combining T-matrix method and the Maxwell-Garnett effective medium theory. And for the aggregates, the diffusion limited aggregation algorithm was used for generating aggregates with different numbers, morphological structures and sizes of spherical monomers, and then the core-mantle Generalized Multi-particle Mie (CMGMM) method was used to compute their scattering parameters.

2. Methodology and model

2.1. T-matrix Method

Owing to the linearity of Maxwell's equations and boundary conditions, the relation between the scattered field coefficients p_{mn} and q_{mn} on one hand and the incident field coefficients a_{mn} and b_{mn} on the other hand is linear and is given by a transition matrix (or T matrix) T as follows:

$$p_{mn} = \sum_{n'=1}^{\infty} \sum_{m'=-n'}^{n'} \left[T^{11}_{mnm'n'} a_{m'n'} + T^{12}_{mnm'n'} b_{m'n'} \right] \tag{1}$$

$$q_{mn} = \sum_{n'=1}^{\infty} \sum_{m'=-n'}^{n'} \left[T^{21}_{mnm'n'} a_{m'n'} + T^{22}_{mnm'n'} b_{m'n'} \right] \tag{2}$$

Eqs. (1) and (2) can be rewritten as

$$\begin{bmatrix} \mathbf{p} \\ \mathbf{q} \end{bmatrix} = \mathbf{T} \begin{bmatrix} \mathbf{a} \\ \mathbf{b} \end{bmatrix} = \begin{bmatrix} \mathbf{T}^{11} & \mathbf{T}^{12} \\ \mathbf{T}^{21} & \mathbf{T}^{22} \end{bmatrix} \begin{bmatrix} \mathbf{a} \\ \mathbf{b} \end{bmatrix} \tag{3}$$

Eq. (3) is the basis of the T-matrix formulation.

2.2. Core-mantle Generalized Multi-sphere Mie-solution Method (CMGMM)

CMGMM method provides a rigorous and complete solution to the lighting scattering problems of core-mantle fractal-like aggregates. The key steps involved in the development of CMGMM method which is similar to GMM method include: (a) expansion of the scattered, internal, and incident electromagnetic fields in terms of vector spherical functions, (b) formation of a linear equation system through the boundary condition at each primary particle in the aggregate, (c) transformation of the

waves scattered by an individual primary particle into the incident waves of the other particles in the aggregate through the addition theorems for vector spherical functions, and (d) solution of the linear system of interactive coefficients.

2.3. Maxwell-Garnett effective medium theory

As the T-matrix method only can be used to simulate the radiative properties of homogenous particles, for the complex aerosol particles, MG effective medium theory is used to obtain the equivalent optical constant of two-component particles, which is defined to satisfy the following relation:

$$\varepsilon_{eff} = \varepsilon_{drop} + \frac{3f\varepsilon_{drop}\left(\varepsilon_{incl} - \varepsilon_{drop}\right)}{\varepsilon_{incl} + 2\varepsilon_{drop} - f\left(\varepsilon_{incl} - \varepsilon_{drop}\right)} \tag{4}$$

where ε_{drop} is the dielectric constant of the drop (mantle), ε_{incl} is the dielectric constant of the inclusion (core), and ε_{eff} is the effective dielectric constant of the composite. f is the volume fraction of the inclusions:

$$f = \left(\frac{r_{incl}}{r_{entire}}\right)^3 = \left(\frac{r_{incl}}{r_{incl} + r_{drop}}\right)^3 \tag{5}$$

Where r_{incl} is the radius of the core, r_{drop} is the thickness of the mantle, and r_{entire} is the radius of the entire particle.

3. Results and discussions

3.1. Single non-spherical particles

According to these previous studies [8-10, 17], we grouped single non-spherical haze particles collected in China into the following four types: mineral particle with water-soluble coating (mineral-WS), organic carbon particle with WS coating (OC-WS), soot particle WS coating (soot-WS) and WS particle with OC coating (WS-OC). Because the relative humidity (RH) is always smaller than 80% when haze events occur, we consider the condition of RH=70% in this paper. The complex refractive indices of WS composition at a RH of 70%, mineral, OC and soot at 1.6μm are 1.391+ 0.0085i, 1.494+ 0.0205i, 1.487+ 0.000048i and 1.778+ 0.468i, respectively, which are interpolated from OPAC database [18]. T-matrix method was combined with the Maxwell-Garnett effective medium theory to calculate the scattering properties of the above four typical haze particles. In this paper, the shape parameters are taken as follows: (a) the ratio of r_{drop} to r_{incl}, q= 0.1 and 0.2; (b) r_{incl}=1, 1.5, 2 and 2.5μm; (c) the spheroid axial ratio a/b=2; cylinder diameter/height ratio D/L=1; Chebyshev particle deformation parameter ε=0.1 and polynomial of degree n=2.

Figure 1 shows the angular distributions of the scattering matrixes for three shapes of OC-WS, mineral-WS, soot-WS and WS-OC with q=0.2, r_{incl}=2μm. Because the scattering matrixes for q=0.1, r_{incl}=2μm is similar to those for q=0.2, r_{incl}=2μm, it is not shown here. The phase function $F_{11}(\Theta)$ (scattering angle, $\Theta \in [0,\pi]$) is the most important element which is proportional to the flux of the scattered light, and satisfies the normalization formulation, $\frac{1}{2}\int_0^{\pi} F11(\Theta)\sin\Theta d\Theta = 1$. The ratio - $F_{12}(\Theta)/F_{11}(\Theta)$ shows the condition of the linear polarization of the scattered light, which can effectively reflect the variation of the polarization. All of these elements which come from the scattering matrix can depict the scattering properties from the intensity, polarization, and the nonsphericity. It can be seen from Figure 1 that the scattering properties of all these four typical particles with different shape parameters are significantly different from each other. Especially, for the same shape, the scattering properties of soot-WS is obvious different from other three particles due to the strong absorption of soot. For each one of the four typical particles, there are variations at different degrees among different shapes. The variation is larger in the region of forward scattering for soot-WS, and in the middle and backward angles for OC-WS, mineral-WS and WS-OC.

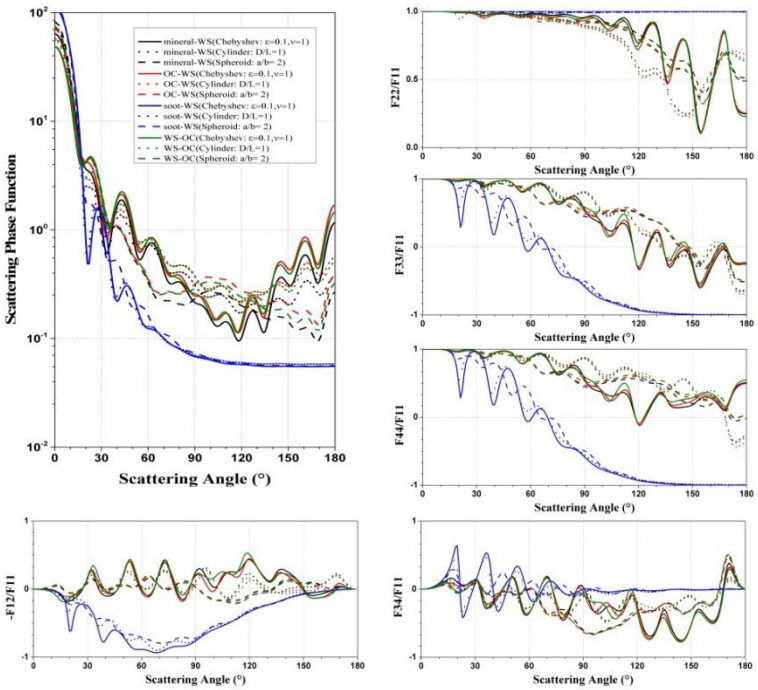

Figure 1. Angular distribution of the scattering matrix based on the four typical single haze particles. The constant parameters are q=0.2, r_{incl}=2μm and λ=1.6μm.

The extinction coefficient (C_{ext}), scattering coefficient (C_{sca}) and single scattering albedo (SSA) of above four types of single non-spherical haze particles are listed in Table 1 with a fixed shape parameter (spheroid, a/b=2). Table 1 depicts that both C_{ext} and C_{sca} increase with q and r_{incl}. In the case of q =0.2, the C_{ext} increases by 31.891, 30.221, 40.179 and 30.951μm^2 when r_{incl} increases from 1 to 2μm for mineral-WS, OC-WS, soot-WS and WS-OC, respectively. The SSA roughly decreases with r_{incl}, but increases with q except for OC-WS. For example, the values of SSA increase by about 0.004 for mineral-WS, OC-WS and WS-OC, but decrease by about 0.03 for soot-WS when q increases from 0.1 to 0.2 for r_{incl}=2μm.

Table 1. Extinction coefficient, scattering coefficient and single scattering albedo of spheroid particle with a/b=2.

	q	r_{incl}(μm)	C_{ext}(μm^2)	C_{sca}(μm^2)	SSA	r_{incl} (μm)	C_{ext}(μm^2)	C_{sca}(μm^2)	SSA
Mineral-WS	0.1	1	14.685	13.430	0.915	2	41.181	32.353	0.786
	0.2	1	17.584	16.175	0.920	2	48.066	37.909	0.789
OC-WS	0.1	1	15.088	14.910	0.988	2	40.758	39.326	0.965
	0.2	1	18.066	17.694	0.979	2	47.915	44.866	0.936
Soot-WS	0.1	1	11.298	5.613	0.497	2	39.942	20.007	0.501
	0.2	1	13.578	6.967	0.513	2	47.146	23.439	0.497
WS-OC	0.1	1	13.998	13.525	0.966	2	44.077	40.310	0.915
	0.2	1	17.827	17.336	0.972	2	48.287	44.405	0.920

3.2. Aggregates

Aggregated particle with complicated geometries is another typical non-spherical aerosol in the atmosphere. Aerosols with this kind of structure are almost soot particles which are commonly formed due to the biomass burning and fuel combustion, and contain ten to hundreds of tiny and nearly spherical particles that join together to form an aggregate. Because soot particles could support surface tension of the water as a film, soot aggregates frequently acquire water coatings in humid air. In this

paper, the fractal-like aggregated particles are simulated using a tunable particle-cluster aggregation method [19]. The fractal-like nature of such aggregates can be mathematically expressed through the following statistical scaling law, $N = k\left(\frac{R_g}{a}\right)^{D_f}$, where N is the number of the monomers in the aggregates, a is the mean radius of the monomers, k is the fractal prefactor, D_f is the fractal dimension, and R_g is the radius of gyration. We used this algorithm to generate fractal aggregates composed of 10, 50 and 90 equal-size monomers with a fixed fractal prefactor (k=1.19) and a fractal dimension (D_f =2.2). Then the CMGMM method was used for calculating the scattering properties of soot aggregate with water-coated monomers. The core radius for each soot-containing monomer is fixed as a_{incl} =15nm, and q=(a- a_{incl})/ a_{incl}.

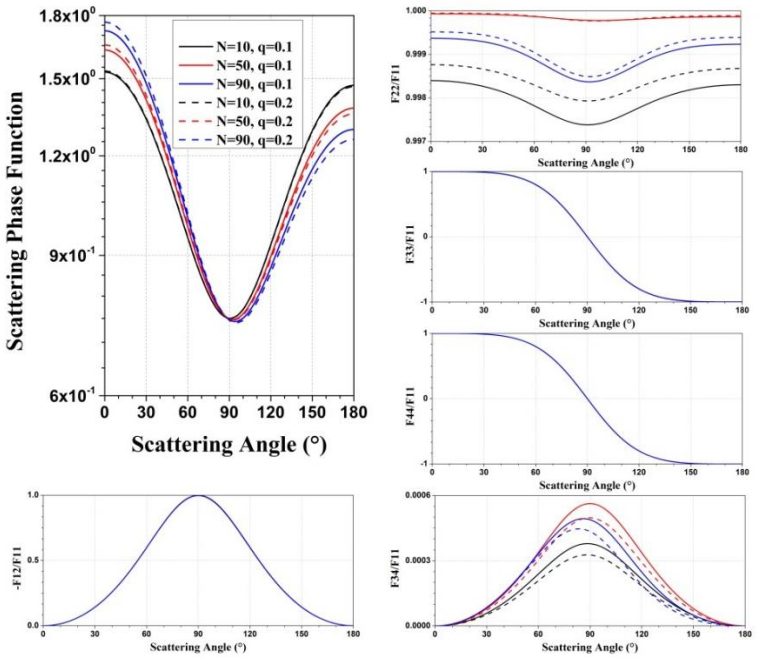

Figure 2. Angular distribution of the scattering matrix for soot aggregates with water coatings. The constant parameters are D_f =2.2, k=1.19 and λ=1.6μm.

Table 2. Extinction coefficient, scattering coefficient and single scattering albedo of soot aggregates with water-coated monomers for N=10, 50, 90, and q=0.1, 0.2.

N	q	C_{ext}(nm^2)	C_{sca}(nm^2)	SSA	N	q	C_{ext}(nm^2)	C_{sca}(nm^2)	SSA
10	0.1	343.8	0.7253	0.0021	10	0.2	350.43	0.9313	0.0027
50	0.1	1754.1	17.1580	0.0098	50	0.2	1790.2	21.7910	0.0122
90	0.1	3221.5	53.1520	0.0165	90	0.2	3287.2	66.7420	0.0203

As shown in Figure 2, the scattering intensities increase with N and q for the forward scattering, however, decrease for the backward scattering. Since the sizes of soot aggregates are relative small, all of elements in the scattering matrix have relative small differences for different morphologies with different N and q. Similar to single non-spherical particles, Table 2 shows that both C_{ext} and C_{sca} increase with size (N) and q. And the value of SSA also increases with N and q. For soot aggregates with 90 monomers, in case of the thickness ratio q increasing from 0.1 to 0.2, the C_{ext}, C_{sca} and SSA

increase 2%, 25.5% and 23%, respectively. For q=0.2, in case of monomer number N = 90, the C_{ext}, C_{sca} and SSA are 7.38, 69.6 and 5.63, respectively, times larger than those for N =10.

4. Conclusions

In this study, the effects of particle size, morphological structure and chemical compositions on the scattering properties for non-spherical and heterogeneous haze particles at a wavelength of 1.6μm were investigated by using T-matrix method and CMGMM method combined with the effective medium theory. Our analysis of numerical results demonstrates that the scattering characteristics are significantly different for both single non-spherical particles and aggregates.

As for single non-spherical particles, the scattering properties of all of mineral-WS, OC-WS, soot-WS and WS-OC with different shape parameters are significantly different from each other. Because of the strong absorption of soot, the scattering properties of soot-WS are obviously different from those of other three type particles with the same shape parameters. As for soot aggregates with water-coated monomers, the scattering phase functions increase with N and q for the forward scattering, however, decrease for the backward scattering. The C_{ext} and C_{sca} of both single non-spherical particles soot aggregates increase with particle size and the thickness ratio. The SSA increases with the thickness ratio for both of them, and it roughly decreases with particle size for single non-spherical particles but increases for soot aggregate with relative small monomer number.

5. Acknowledgments

The authors appreciate financial support for this work from the Key Program of the National Natural Science Foundation of China (Grant No. 41130528) and the Strategic Priority Research Program of the Chinese Academy of Sciences (Grant No. XDB05020100). We thank Dr. Michael Mishchenko for publicly providing the T-matrix code, and thank Dr. Yunlin Xu for publicly providing the CMGMM code.

References

[1] Baker D F, Doney S C and Schimel D S 2006 *Tellus B* **58** 359-365
[2] Chevallier F, Bréon F-M and Rayner P J 2007 *J. Geophys. Res.* **112** 1-11
[3] Feng L, Palmer P I, Bösch H and Dance S 2009 *Atmos. Chem. Phys.* **9** 2619-2633
[4] Aben I, Hasekamp O and Hartmann W 2007 *J. Quant. Spectrosc. Radiat. Transfer.* **104** 450-459
[5] Mao J and Kawa S R 2004 *Appl. Opt.* **43** 914-927
[6] Che H, Zhang X, Li Y, Zhou Z, Qu J and Hao X 2009 *Theor. Appl. Climatol.* **97** 235-242
[7] Zhang X Y, Wang Y Q, Niu T, Zhang X C, Gong S L, Zhang Y M and Sun J Y 2012 *Atmos. Chem. Phys.* **12** 779-799
[8] Li W J and Shao L Y 2009 *Atmos. Chem. Phys.* **9** 1863-1871
[9] Li W J, Shao L Y and Buseck P R 2010 *Atmos. Chem. Phys.* **10** 8119-8130
[10] Li W J, Zhang D Z, Shao L Y, Zhou S Z and Wang W X 2011 *Atmos. Chem. Phys.* **11** 11733-11744
[11] Mishchenko M I, Travis L D and Mackowski D W 1996 *J Quant Spectrosc Radiat Transfer* **55** 535-575
[12] Sun W, Fu Q and Chen Z 1999 *Appl. Opt.* **38** 3141-3151
[13] Mishchenko M I 1991 *J. Opt. Soc. Am. A* **8** 871-882
[14] Xu Y-l 1995 *Appl. Opt.* **34** 4573-4588
[15] Ari H S and Olli P M P 1996 *J. Phys. D: Appl. Phys.* **29** 514
[16] Xu Y-l and Khlebtsov N G *J. Quant. Spectrosc. Radiat. Transfer.* **79–80** 1121-1137
[17] Li W and Shao L 2009 *J Geophys Res* **114** D09302
[18] Hess M, Koepke P and Schult I 1998 *Bulletin of the American Meteorological Society* **79** 831-844
[19] Filippov A V, Zurita M and Rosner D E 2000 *J. Colloid. Interf. Sci* **229** 261-273